

Finite Element Methods for Suspension Bridge Models

B. SEMPER

University of Texas at Arlington
 Box 19408, Arlington, Texas 76019-0408, U.S.A.

(Received May 1992; revised and accepted September 1992)

Abstract—A fourth order integro-differential equation used to model static deflection in suspension bridges is examined. Galerkin approximation methods are presented and analyzed, as well as methods for solving the resulting system of equations. Numerical experiments are presented.

1. INTRODUCTION

The deflection theory for suspension bridges was originally developed by Melan [1] in the late 1880's. This model is mostly used for large scale simulation of bridge deflection and resulting stresses and strains due to live loads. The classical model, which we shall analyze, makes several assumptions about the structure:

- (1) The cables can slide freely through “saddles” atop the towers (although the case when the cables are anchored atop the towers is easily adopted);
- (2) The support towers are nonbending; and
- (3) The “hangers” connecting the cables to the bridge deck are unextendible (thus, any deflection in the stiffening girder is matched by a deflection in the cables).

We note that assumption (3) is not valid in the case of large scale oscillations in the bridge deck, and recent works by Lazur and McKenna [2] and Choi, Jen, and McKenna [3] indicate interesting nonlinear effects if extendible hangers are considered.

Consider a three span suspension bridge (Figure 1). We assume the left end of the bridge to be located at the point $x = 0$, and take downward to be the positive direction. The live load on the bridge deck is given by the function $p(x)$, assumed to be positive, and the deflection in the i^{th} span of the bridge is denoted by the function $v_i(x)$. The system of equations used to model this deflection (see [4] or [5] for the derivation) is then given by, for $i = 1, 2, 3$,

$$EI v_i^{(\text{iv})} - (H_g + H_p) v_i'' = p(x) - \frac{w}{H_g} H_p, \quad (1.1)$$

where

$$H_p = \frac{E_c A_c}{L_c} \left(\frac{w}{H_g} \right) \sum_{i=1}^3 \int_{\ell_i} v_i(x) dx.$$

Here, E is the modulus of elasticity and I the moment of inertia of the stiffening girders (assumed constant throughout the bridge for simplicity, although the theory we develop is easily extended to the case for nonconstant E and I), w is the dead load weight of the bridge deck itself, and H_g is the horizontal tension created in the cables by this dead load (and assumed constant

Typeset by $\mathcal{A}\mathcal{M}\mathcal{S}\text{-}\mathcal{T}\mathcal{E}\mathcal{X}$

throughout the structure due to assumption (1) above). The relationship

$$\frac{w}{H_g} = \frac{8f_i}{\ell_i^2}, \quad i = 1, 2, 3, \quad (1.2)$$

can be used to find this horizontal tension (see, e.g., [4]) where f_i is the sag in the i^{th} span and ℓ_i is the length of the i^{th} span (see Figure 1). E_c and A_c are the modulus of elasticity and cross sectional area of the cable, respectively, and L_c is a length given by the integral

$$L_c = \int_0^\ell \left(\frac{ds}{dx} \right) dx, \quad \ell = \ell_1 + \ell_2 + \ell_3. \quad (1.3)$$

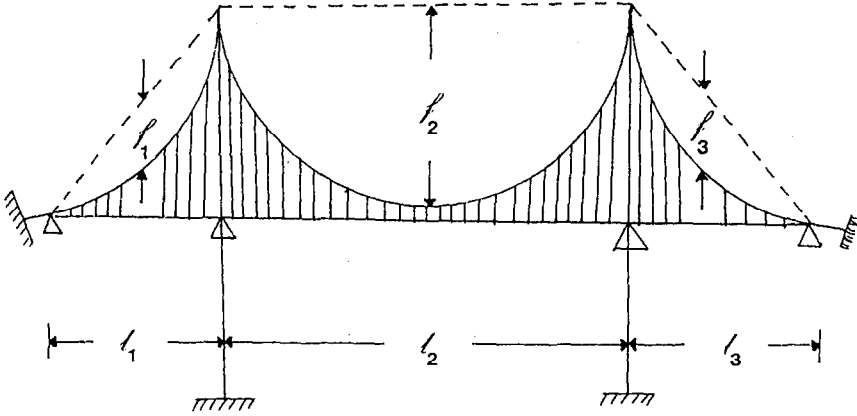


Figure 1. Three span suspension bridge.

The term H_p is the horizontal tension in the cable created by the live load, and acts as a restoring force in (1.1). In some models, this term is taken to be zero (unextendible cables), which leads to a simple fourth order ordinary differential equation. If the cables are assumed to be anchored at the top of the towers, H_p is computed for each span separately, and the sum in (1.1) is not used (the tension in each span being computed by the integral of $v_i(x)$ for that particular span). If the live load is relatively small compared to the dead load, it is assumed that $H_p \ll H_g$, and hence the equation can be linearized by replacing the $(H_g + H_p)$ term in (1.1) with just H_g . This leads to a "less stiff" model, and stress/strain computations done with this model would be considered conservative. We will examine this linear model, although the numerical techniques we will develop will be applied to the nonlinear equation as well, in Section 6, with mixed result.

Let us denote the deflection in the entire bridge by $V(x)$, where $V(x) = v_i(x)$ on the i^{th} span. The boundary conditions associated with (1.1) depend upon the type of bridge being modeled: for a *hinged bridge*, we have that $V(x) = V''(x) = 0$ at the ends of each span, while for a *continuous span bridge*, it is assumed that $V(x) = V''(x) = 0$ at $x = 0, \ell$, $V(x) = 0$ at the ends of the spans, and that $V'(x)$ and $V''(x)$ are continuous across the tower nodes (i.e., $V(x) \in C^2(0, \ell)$). We will examine both of these models.

Several methods for approximating this model have appeared in the engineering literature [6]. Most of these methods depend upon the use of the Laplace transform, and as such are limited by the inversion process for the transform method. Another numerical approach to this type of ordinary integro-differential equation was studied by Fairweather and Saylor [7]. Their method involved transforming the equation to "classical form" by adding another variable and another differential equation; the resulting system was then approximated using a collocation finite element method.

In this paper, we will present a simple finite element (h -method) approach to this problem; the drawback to this approach is that the resulting stiffness matrix would normally be full, but we

will develop an iteration procedure to circumvent this difficulty. This approach is easy to apply and carries with it all the flexibility of the finite element method; the results can also be extended to nonuniform (variable coefficient) models. In Section 2, we present the mathematical model and derive some basic bounds for the solution. In Section 3, we analyze conforming and mixed finite element methods for the problem, and present error bounds. Section 4 deals with the iteration process used to solve the resulting matrix equation; we analyze the standard iteration and also a modified, more robust technique. Some comments on numerical implementation and the nonlinear problem appear in Section 5, and in Section 6, we present some numerical experiments involving the methods of the previous sections.

We will utilize the following notation: the Sobolev space of all L^2 functions with k derivatives in L^2 on $(0, L)$ will be denoted by H^k , with \mathring{H}^k being all such functions which vanish along with their first $(k - 1)$ derivatives at $x = 0, L$. We denote the L^2 inner product by

$$(f, g) = \int_0^L f(x) g(x) dx,$$

and the L^2 norm will be denoted by

$$\|f\| = \left(\int_0^L f^2(x) dx \right)^{1/2}.$$

The norm on H^k is denoted by

$$\|f\|_k = \left(\sum_{j=0}^k \left\| \frac{d^j f}{dx^j} \right\|^2 \right)^{1/2}.$$

We denote the dual space of \mathring{H}^k by H^{-k} with the norm

$$\|f\|_{-k} = \sup_{\substack{\phi \in \mathring{H}^k \\ \|\phi\|_k = 1}} \langle f, \phi \rangle,$$

where $\langle \cdot, \cdot \rangle$ represents the duality pairing. We will also make use of the Poincaré inequality; namely, if $f \in \mathring{H}^1$, then

$$\|f\| \leq L \|f'\|. \quad (1.4)$$

2. THE MATHEMATICAL MODEL

We now present the mathematical model which we will analyze in this work. For simplicity, we will consider the equation over only one span, although in Section 5 we indicate how our methods can be applied to model an entire three span bridge. Consider the linear ordinary integro-differential equation

$$\begin{aligned} C_1 v^{(iv)} - v'' + C_2 \int_0^L v(x) dx &= p(x), \\ v(0) = v''(0) = v(L) = v''(L) &= 0, \end{aligned} \quad (2.1)$$

where C_1 and C_2 are positive constants. The standard variational formulation of (2.1) is given by the following.

Find $v(x) \in H^2 \cap \mathring{H}^1$ so that

$$B(v, \psi) \equiv C_1 (v'', \psi'') + (v', \psi') + C_2 \left[\int_0^L v(x) dx \right] \left[\int_0^L \psi(x) dx \right] = P(\psi) \equiv \langle p, \psi \rangle, \quad (2.2)$$

for all $\psi \in H^2 \cap \mathring{H}^1$.

We note that the $v''(x)$ boundary condition is a natural boundary condition in this setting.

REMARK 2.1. Throughout this work we will make use of several constants, and denote these generically by K , or K_1 , K_2 if more than one are needed. We shall reserve C_1 , C_2 for the constants appearing in (2.1).

LEMMA 2.1. *If $p(x) \in H^{-2}$, then problem (2.2) has a unique solution.*

PROOF. The result follows from the Lax-Milgram theorem as soon as we show $B(\cdot, \cdot)$ is continuous and elliptic. Note that by the Cauchy-Schwarz inequality, if $(v, \psi) \in [H^2 \cap \mathring{H}^1] \times [H^2 \cap \mathring{H}^1]$, then

$$\begin{aligned} B(v, \psi) &= C_1(v'', \psi'') + (v', \psi') + C_2 \left[\int_0^L v(x) dx \right] \left[\int_0^L \psi(x) dx \right] \\ &\leq C_1 \|v''\| \|\psi''\| + \|v'\| \|\psi'\| + C_2 L \|v\| \|\psi\| \leq K \|v\|_2 \|\psi\|_2, \end{aligned} \quad (2.3)$$

and hence $B(\cdot, \cdot)$ is continuous on $[H^2 \cap \mathring{H}^1] \times [H^2 \cap \mathring{H}^1]$. Also, if $v \in H^2 \cap \mathring{H}^1$, the Poincaré inequality shows

$$\begin{aligned} B(v, v) &= C_1 \|v''\|^2 + \|v'\|^2 + C_2 \left[\int_0^L v(x) dx \right]^2 \\ &\geq C_1 \|v''\|^2 + \|v'\|^2 \geq C_1 \|v''\|^2 + \frac{1}{2} \|v'\|^2 + \frac{1}{2L^2} \|v\|^2 \geq K \|v\|_2^2. \end{aligned} \quad (2.4)$$

The result follows. ■

It is rather straightforward to derive regularity results for the solution of (2.1). The following result will be useful in the error analysis of the finite element methods:

LEMMA 2.2. *Suppose $p(x) \in H^{-k}$ and $v(x)$ is the solution of (2.1). Then there exists a constant K_k dependent on C_1 , C_2 , and L , such that*

$$\|v\|_{4-k} \leq K_k \|p\|_{-k}, \quad k = 0, 1, 2. \quad (2.5)$$

PROOF. The result follows easily for $k = 2$ by the ellipticity of $B(\cdot, \cdot)$. If $k = 1$, we let $\psi = -v''$ in (2.2) and note after integrating by parts

$$\begin{aligned} C_1 \|v'''\|^2 + \|v''\|^2 &= -\langle p, v'' \rangle + C_2 \left[\int_0^L v(x) dx \right] \left[\int_0^L v''(x) dx \right] \\ &\leq \|p\|_{-1} \|v''\|_1 + C_2 L \|v\| \|v''\|. \end{aligned} \quad (2.6)$$

The result follows after applying the arithmetic/geometric mean inequality and the previous bound. If $k = 0$, we can use (2.1) to bound $\|v^{(iv)}\|$ by the previous bounds, and again the result follows. ■

REMARK 2.2. We will assume that C_1 is $O(1)$ to avoid the pitfalls of a singular perturbation problem (see, e.g., [8]). For the suspension bridge model, $C_1 = EI/H_g$, and is generally $O(1)$. If, however, we transform the equation to dimensionless variables, then $C_1 = EI/(H_g L^4)$, which may be small for a long span bridge. We shall keep the analysis simple by assuming the problem to be posed on the interval $(0, L)$, and assuming (in Section 3) that enough grid points are employed in our numerical method.

A simpler formulation of the problem can be formulated as follows: we note that (2.1) can be rewritten as the following system:

$$\begin{aligned} -C_1 \phi'' - v'' + C_2 \int_0^L v(x) dx &= p(x), \\ -v'' &= \phi, \\ v(0) = v(L) = \phi(0) = \phi(L) &= 0. \end{aligned} \quad (2.7)$$

The variational formulation of this problem is given by the following:

$$\begin{aligned} &\text{Given } (p, g) \in \mathring{H}^{-1} \times \mathring{H}^{-1}, \text{ find } (v, \phi) \in \mathring{H}^1 \times \mathring{H}^1 \text{ so that} \\ &a(v, \psi) + b(\phi, \psi) = \langle p, \psi \rangle, \quad \text{for all } \psi \in \mathring{H}^1, \\ &b(v, \eta) - d(\phi, \eta) = \langle g, \eta \rangle, \quad \text{for all } \eta \in \mathring{H}^1, \end{aligned} \quad (2.8)$$

where

$$\begin{aligned} a(v, \psi) &\equiv (v', \psi') + C_2 \left[\int_0^L v(x) dx \right] \left[\int_0^L \psi(x) dx \right], \\ b(v, \eta) &\equiv C_1 (v', \eta'), \\ d(\phi, \eta) &\equiv C_1 (\phi, \eta). \end{aligned} \quad (2.9)$$

The problem is thus reduced to a mixed method formulation of the type first studied by Babuska [9] and Brezzi [10], in this case generalized by the addition of the auxiliary form $d(\cdot, \cdot)$. This generalization is mentioned by Roberts and Thomas (see Remark 10.8 in [11]) and analyzed in some detail by Brezzi and Fortin [12]. Due to the choice of bilinear forms (2.9) and the fact that both $v(x)$ and $\phi(x)$ are to be found in the same space, problem (2.8) is much easier to analyze than the general mixed method problem. The following result is proved in more generality by Brezzi and Fortin (see Theorem 1.2 in [12]), and our proof is a simplification of their proof.

LEMMA 2.3. *Problem (2.8) has a unique solution, and in fact if $(p, g) \in H^{-k} \times H^{-k}$, $k = 0, 1$, there exists a constant K such that*

$$\|v\|_{2-k} + \|\phi\|_{2-k} \leq K \left(\|p\|_{-k} + \|g\|_{-k} \right). \quad (2.10)$$

PROOF. Suppose first $k = 1$. We define the linear operators A , B , and D from \mathring{H}^1 to \mathring{H}^{-1} by

$$\langle A u, \psi \rangle = a(u, \psi), \quad \langle B u, \psi \rangle = b(u, \psi), \quad \langle D u, \psi \rangle = d(u, \psi), \quad (2.11)$$

for all $u, \psi \in \mathring{H}^1$. Then (2.8) can be written as

$$\begin{aligned} &\text{Find } (v, \phi) \in \mathring{H}^1 \times \mathring{H}^1 \text{ so that} \\ &A v + B \phi = p, \quad \text{in } \mathring{H}^{-1}, \\ &B v + D \phi = g, \quad \text{in } \mathring{H}^{-1}. \end{aligned} \quad (2.12)$$

If A , B , and D are invertible, it is clear that (2.12) has a unique solution. Note that for any $u, \psi \in \mathring{H}^1$,

$$\begin{aligned} a(u, \psi) &= (u', \psi') + C_2 \left[\int_0^L u(x) dx \right] \left[\int_0^L \psi(x) dx \right] \\ &\leq \|u'\| \|\psi'\| + C_2 \left[\int_0^L |u(x)| dx \right] \left[\int_0^L |\psi(x)| dx \right] \\ &\leq \|u'\| \|\psi'\| + L C_2 \|u\| \|\psi\| \leq \max\{1, L C_2\} \|u\|_1 \|\psi\|_1, \end{aligned} \quad (2.13)$$

and also, by the Poincaré inequality,

$$a(\psi, \psi) = (\psi', \psi') + C_2 \left[\int_0^L \psi(x) dx \right]^2 \geq \|\psi'\|^2 \geq \min \left\{ \frac{1}{2}, \frac{1}{2L^2} \right\} \|\psi\|_1^2. \quad (2.14)$$

It is equally easy to see that

$$b(u, \psi) \leq C_1 \|u\|_1 \|\psi\|_1, \quad (2.15)$$

$$b(\psi, \psi) \geq C_1 \min \left\{ \frac{1}{2}, \frac{1}{2L^2} \right\} \|\psi\|_1^2,$$

(thus, the inf-sup condition is trivial) and

$$d(u, \psi) \leq C_1 \|u\| \|\psi\| \leq C_1 \|u\|_1 \|\psi\|_1, \quad (2.16)$$

$$d(\psi, \psi) = C_1 \|\psi\|^2 \geq 0.$$

From (2.13)–(2.15), we know that A and B are invertible. Also, D is continuous from (2.16), but since the bilinear form $d(\cdot, \cdot)$ does not coerce the \mathring{H}^1 norm, we do not know that D is invertible; it is, however, positive for nonzero $\psi(x)$. The proof now proceeds by regularizing the problem: denote the \mathring{H}^1 inner product by $((\cdot, \cdot))$. We then consider the following problem (for $0 < \epsilon < 1$):

$$\begin{aligned} &\text{Given } (p, g) \in \mathring{H}^{-1} \times \mathring{H}^{-1}, \text{ find } (v_\epsilon, \phi_\epsilon) \in \mathring{H}^1 \times \mathring{H}^1 \text{ so that} \\ &\epsilon((v_\epsilon, \psi)) + a(v_\epsilon, \psi) + b(\phi_\epsilon, \psi) = \langle p, \psi \rangle, \quad \text{for all } \psi \in \mathring{H}^1, \end{aligned} \quad (2.17)$$

$$b(v_\epsilon, \eta) - \epsilon((\phi_\epsilon, \eta)) - d(\phi_\epsilon, \eta) = \langle g, \eta \rangle, \quad \text{for all } \eta \in \mathring{H}^1.$$

We note that (2.17) is of the form (2.12), where all operators are invertible (due to the positivity of the form $d(\cdot, \cdot)$), and hence a unique solution $(v_\epsilon, \phi_\epsilon)$ exists. We now show that v_ϵ and ϕ_ϵ can be bounded independently of ϵ , and then appeal to a limiting argument. If we set $\psi = v_\epsilon$ and $\eta = \phi_\epsilon$ in (2.17), and then subtract the two equations (using the fact that $b(\cdot, \cdot)$ is symmetric), we have

$$\epsilon \|v_\epsilon\|_1^2 + \epsilon \|\phi_\epsilon\|_1^2 + a(v_\epsilon, v_\epsilon) + d(\phi_\epsilon, \phi_\epsilon) = \langle p, v_\epsilon \rangle - \langle g, \phi_\epsilon \rangle. \quad (2.18)$$

It now follows from inequalities (2.13)–(2.16) and equations (2.17) that

$$\begin{aligned} \|\phi_\epsilon\|_1^2 &\leq K_1 b(\phi_\epsilon, \phi_\epsilon) \leq K_1 |\langle p, \phi_\epsilon \rangle - a(v_\epsilon, \phi_\epsilon) - \epsilon((v_\epsilon, \phi_\epsilon))| \\ &\leq K_1 [\|p\|_{-1} + \|v_\epsilon\|_1 + \epsilon \|v_\epsilon\|_1] \|\phi_\epsilon\|_1, \end{aligned} \quad (2.19)$$

and also

$$\begin{aligned} \|v_\epsilon\|_1^2 &\leq K_2 b(v_\epsilon, v_\epsilon) \leq K_2 |\langle g, v_\epsilon \rangle + \epsilon((\phi_\epsilon, v_\epsilon)) + d(\phi_\epsilon, v_\epsilon)| \\ &\leq K_2 [\|g\|_{-1} + \epsilon \|\phi_\epsilon\|_1 + \|\phi_\epsilon\|_1] \|v_\epsilon\|_1. \end{aligned} \quad (2.20)$$

By way of (2.18)–(2.20), we now have

$$\begin{aligned} \epsilon \|\phi_\epsilon\|_1^2 + C_1 \|\phi_\epsilon\|^2 &\leq \|p\|_{-1} \|v_\epsilon\|_1 + \|g\|_{-1} \|\phi_\epsilon\|_1 \\ &\leq \|p\|_{-1} \|v_\epsilon\|_1 + K_1 \|g\|_{-1} \left\{ \|p\|_{-1} + (1 + \epsilon) \|v_\epsilon\|_1 \right\} \\ &= \left\{ \|p\|_{-1} + 2K_1 \|g\|_{-1} \right\} \|v_\epsilon\|_1 + K_1 \|g\|_{-1} \|p\|_{-1} \\ &\leq K_2 \left\{ \|p\|_{-1} + 2K_1 \|g\|_{-1} \right\} \left\{ \|g\|_{-1} + \epsilon \|\phi_\epsilon\|_1 + \|\phi_\epsilon\|_1 \right\} + K_1 \|g\|_{-1} \|p\|_{-1}. \end{aligned} \quad (2.21)$$

Applications of the arithmetic/geometric mean inequality then give

$$\sqrt{\epsilon} \|\phi_\epsilon\|_1 + \|\phi_\epsilon\|_1 \leq \bar{K} \left(\|p\|_{-1} + \|g\|_{-1} \right), \quad (2.22)$$

with \bar{K} dependent on K_1 and K_2 , but not ϵ . We can use (2.20) and then (2.19) to obtain

$$\begin{aligned} \|v_\epsilon\|_1 &\leq \bar{K}_1 \left(\|p\|_{-1} + \|g\|_{-1} \right), \\ \|\phi_\epsilon\|_1 &\leq \bar{K}_2 \left(\|p\|_{-1} + \|g\|_{-1} \right), \end{aligned} \quad (2.23)$$

where both \bar{K}_1, \bar{K}_2 are independent of ϵ , but may depend on C_1, C_2 , and L . The proof now concludes by letting ϵ go to zero. The bounds for the case $k = 0$ follow from the above bounds and the differential equations (2.7). ■

3. FINITE ELEMENT APPROXIMATION

We now proceed to discretize problems (2.2) and (2.8). Suppose we have a partition of $[0, L]$ given by

$$0 = x_0 < x_1 < x_2 < \cdots < x_{N-1} < x_N = L, \quad (3.1)$$

such that the grid is quasi-uniform: denoting $h_j = x_j - x_{j-1}$, and $h = \max\{h_j\}$, we assume the existence of constants c, C , independent of h , so that, for $0 < h < 1$,

$$ch \leq h_j \leq Ch, \quad j = 1, 2, \dots, N. \quad (3.2)$$

We first approximate the solution of (2.2). Let S_c^h denote the space of piecewise polynomials on the above grid such that $S_c^h \subseteq H^2 \cap \mathring{H}^1$; such functions can easily be constructed in one dimension by using, for example, cubic B -splines (see e.g., [13]). The following approximation property is well known (see, e.g., [14]): if $v \in H^m$, then there exists a $\chi \in S_c^h$ such that

$$\|v - \chi\|_k \leq K h^{m-k} \|v\|_m, \quad (3.3)$$

where K is independent of $v(x)$ and h , and $0 \leq k \leq m \leq R + 1$, R being the degree of the piecewise polynomials which make up S_c^h (in this case $R = 3$).

The finite element formulation of (2.2) thus becomes the following.

Find $v_h \in S_c^h$ such that

$$B(v_h, \psi) = \langle p, \psi \rangle, \quad \text{for all } \psi \in S_c^h. \quad (3.4)$$

We will refer to (3.4) as the *conforming method* and (when the model calls for a multi-span bridge) use it to approximate the continuous span bridge model.

THEOREM 3.1. *Problem (3.4) has a unique solution, and further, if $v(x)$ is the solution of (2.2), there exist constants K_1, K_2 independent of h such that*

$$\|v - v_h\|_2 \leq K_1 \inf_{\chi \in S_c^h} \{\|v - \chi\|_2\}, \quad (3.5)$$

$$\left| \int_0^L v(x) dx - \int_0^L v_h(x) dx \right| \leq K_2 h^2 \|v - v_h\|_2. \quad (3.6)$$

PROOF. Since $B(\cdot, \cdot)$ is symmetric and elliptic on $(H^2 \cap \mathring{H}^1) \times (H^2 \cap \mathring{H}^1)$, it follows that the stiffness matrix generated by (3.4) is symmetric positive definite, and hence, (3.4) is uniquely solvable. Further, by (2.2) and (3.4), we see

$$B(v - v_h, \chi) = 0, \quad \text{for all } \chi \in S_c^h. \quad (3.7)$$

Using this fact, along with (2.3) and (2.4), we have, for any $\chi \in S_c^h$,

$$\|v - v_h\|_2^2 \leq K B(v - v_h, v - v_h) = K B(v - v_h, v - \chi) \leq K_1 \|v - v_h\|_2 \|v - \chi\|_2, \quad (3.8)$$

and (3.5) follows. To show (3.6), we first note

$$\left| \int_0^L v(x) dx - \int_0^L v_h(x) dx \right| \leq \sqrt{L} \|v - v_h\|. \quad (3.9)$$

We now proceed to bound $\|v - v_h\|$ by using the standard duality argument: for simplicity, denote $e_h(x) = v(x) - v_h(x) \in H^2 \cap \mathring{H}^1$. Letting $p(x) = e_h(x) = \psi(x)$ in (2.2) and using (3.7) gives, for $\chi(x)$ as in (3.3),

$$\begin{aligned} \|e_h\|^2 &= B(v, e_h) = B(v - \chi, e_h) \leq K \|v - \chi\|_2 \|e_h\|_2 \\ &\leq K h^2 \|v\|_4 \|e_h\|_2 \leq K_2 h^2 \|e_h\| \|e_h\|_2, \end{aligned} \quad (3.10)$$

the last inequality following from the regularity result (2.5). This shows (3.6). ■

REMARK 3.1. The arguments of (2.3) and (2.4) show that the energy norm for the problem, defined by

$$\|v\| = \sqrt{B(v, v)}, \quad (3.11)$$

is equivalent to the H^2 norm, and hence, (3.5) holds for the energy norm as well. Combining (3.5), (3.3), and the regularity result (2.5), we see that the finite element error in the H^2 norm (or for that matter the energy norm) is $O(h^{2-k})$, provided $f \in H^{-k}$, $k = 0, 1, 2$, whereas the error given by (3.6) would be $O(h^{4-k})$.

To formulate the finite element approximation to (2.8), we need to construct a space of piecewise polynomials $S^h \subseteq \dot{H}^1$. In this case, the only requirement on the functions is that they be continuous, e.g., piecewise linears or quadratics. The same approximation property (3.3) holds. The numerical problem then becomes

$$\begin{aligned} &\text{Find } (v_h, \phi_h) \in S^h \times S^h \text{ such that} \\ &a(v_h, \psi) + b(\phi_h, \psi) = \langle p, \psi \rangle, \quad \text{for all } \psi \in S^h, \\ &b(v_h, \eta) - d(\phi_h, \eta) = \langle g, \eta \rangle, \quad \text{for all } \eta \in S^h. \end{aligned} \quad (3.12)$$

We note that for our particular problem, the function $g(x)$ would be taken to be zero. We will refer to (3.12) as the *mixed formulation*, and in multi-span computations this formulation will be used for the hinged bridge model. We then have the following result, which again shows quasi-optimal convergence for the finite element solution:

THEOREM 3.2. *Problem (3.12) has a unique solution, and if (v, ϕ) is the solution of (2.8), then there exists a constant K independent of h such that*

$$\|\phi - \phi_h\|_1 + \|v - v_h\|_1 \leq K \left\{ \inf_{\chi \in S^h} \|\phi - \chi\|_1 + \inf_{\psi \in S^h} \|v - \psi\|_1 \right\}. \quad (3.13)$$

PROOF. The result is again due to Brezzi and Fortin; the proof is identical to the proof of Proposition 2.11 in [12], and hence omitted. \blacksquare

We finally note that by the approximation property (3.3) (assuming our approximation space is made up of piecewise linears) and the regularity result (2.10), we have that $p \in H^{-k}$ implies the error in (3.13) is $O(h^{1-k})$, $k = 0, 1$. An error bound similar to (3.6) is possible using a duality argument, and the rate of convergence would be $O(h^{2-k})$.

4. SOLVING THE SYSTEM OF EQUATIONS

We now consider iterative methods to solve the system of equations generated by the finite element discretization (3.12). We first note that (3.12) may be rewritten as

$$\begin{aligned} &\text{Find } (v_h, \phi_h) \in S^h \times S^h \text{ such that} \\ &C_1(\phi'_h, \psi') + (\phi_h, \psi) + C_2 \left[\int_0^L v_h(x) dx \right] \left[\int_0^L \psi(x) dx \right] = \langle p, \psi \rangle, \quad \text{for all } \psi \in S^h, \\ &(v'_h, \eta') = (\phi_h, \eta), \quad \text{for all } \eta \in S^h. \end{aligned} \quad (4.1)$$

The integral terms in (4.1) will result in a block matrix with one full block if the method is implemented in the standard way. For a large bridge, our discretization may require N to be on the order of 10^4 , thus making the prospect of forming the full matrix impossible. The following

iteration scheme can be used to avoid this difficulty:

$$\begin{aligned}
\mathcal{S}_p^0 &= 0, \\
\text{For } k = 0, 1, \dots, \text{ find } (\phi_h^{k+1}, v_h^{k+1}) &\in S^h \times S^h \text{ so that} \\
C_1 \left((\phi_h^{k+1})', \psi' \right) + (\phi_h^{k+1}, \psi) &= \langle p, \psi \rangle - C_2 (\mathcal{S}_p^k, \psi), \quad \text{for all } \psi \in S^h, \\
\left((v_h^{k+1})', \eta' \right) &= (\phi_h^{k+1}, \eta), \quad \text{for all } \eta \in S^h, \\
\mathcal{S}_p^{k+1} &= \int_0^L v_h^{k+1}(x) dx.
\end{aligned} \tag{4.2}$$

We now prove a convergence result for this algorithm:

THEOREM 4.1. *Let (ϕ_h, v_h) be the solution of (4.1), and suppose $C_2 L^3 < 1$. Then the sequence (ϕ_h^k, v_h^k) generated by (4.2) converges to (ϕ_h, v_h) in $\dot{H}^1 \times \dot{H}^1$.*

PROOF. Notate $\tilde{\mathcal{S}}_p = \int_0^L v_h(x) dx$. Then

$$\left| \tilde{\mathcal{S}}_p - \mathcal{S}_p^{k+1} \right| \leq \int_0^L |(v_h - v_h^{k+1})(x)| dx \leq \sqrt{L} \|v_h - v_h^{k+1}\| \leq L^{3/2} \|(v_h - v_h^{k+1})'\|. \tag{4.3}$$

By (4.1) and (4.2), we note

$$\left((v_h - v_h^{k+1})', \eta' \right) = ((\phi_h - \phi_h^{k+1}), \eta), \quad \text{for all } \eta \in S^h, \tag{4.4}$$

so that

$$\begin{aligned}
\|(v_h - v_h^{k+1})'\|^2 &= ((\phi_h - \phi_h^{k+1}), (v_h - v_h^{k+1})) \\
&\leq \|\phi_h - \phi_h^{k+1}\| \|v_h - v_h^{k+1}\| \leq L \|\phi_h - \phi_h^{k+1}\| \|(v_h - v_h^{k+1})'\|.
\end{aligned} \tag{4.5}$$

Combining (4.3) and (4.5), we now have

$$\left| \tilde{\mathcal{S}}_p - \mathcal{S}_p^{k+1} \right| \leq L^{5/2} \|\phi_h - \phi_h^{k+1}\|. \tag{4.6}$$

Likewise, since $(\phi_h - \phi_h^{k+1})(x) \in S^h$, we have from (4.1) and (4.2) that

$$\begin{aligned}
C_1 \left\| (\phi_h - \phi_h^{k+1})' \right\|^2 + \|\phi_h - \phi_h^{k+1}\|^2 &= C_1 \left((\phi_h - \phi_h^{k+1})', (\phi_h - \phi_h^{k+1})' \right) \\
&\quad + (\phi_h - \phi_h^{k+1}, \phi_h - \phi_h^{k+1}) = -C_2 (\tilde{\mathcal{S}}_p - \mathcal{S}_p^k) \int_0^L (\phi_h - \phi_h^{k+1})(x) dx \\
&\leq C_2 \left| \tilde{\mathcal{S}}_p - \mathcal{S}_p^k \right| \int_0^L |(\phi_h - \phi_h^{k+1})(x)| dx \leq \sqrt{L} C_2 \left| \tilde{\mathcal{S}}_p - \mathcal{S}_p^k \right| \|\phi_h - \phi_h^{k+1}\|.
\end{aligned} \tag{4.7}$$

By way of (4.6) and (4.7), we then have

$$\left| \tilde{\mathcal{S}}_p - \mathcal{S}_p^{k+1} \right| \leq L^3 C_2 \left| \tilde{\mathcal{S}}_p - \mathcal{S}_p^k \right|, \tag{4.8}$$

and so $\mathcal{S}_p^k \rightarrow \tilde{\mathcal{S}}_p$ in \mathbb{R}^1 by our assumption on $L^3 C_2$. It then follows from (4.7) that $\phi_h^k \rightarrow \phi_h$ in \dot{H}^1 and hence from (4.5) that $v_h^k \rightarrow v_h$ in \dot{H}^1 . \blacksquare

REMARK 4.1. Relating the constant C_2 to the suspension bridge model (1.1), the condition that $L^3 C_2 < 1$ becomes

$$\frac{L^3 E_c A_c w^2}{H_g^3 L_c} < 1. \tag{4.9}$$

Using the identity (1.2), (where f is now the sag in the span we are modeling), this becomes

$$\left(\frac{f}{L}\right)^3 < \frac{w L_c}{512 E_c A_c}. \quad (4.10)$$

The ratio f/L is called the *dip-span ratio* of the bridge (or span). Thus, we can say the iteration scheme (4.2) will converge if the dip-span ratio is small enough, or, from (4.9), the dead load horizontal tension H_g is large enough. We also note that the iterative scheme presented in Theorem 4.1 can easily be adopted for the conforming method (3.4), and the same proof works with minor modifications.

We now present a more robust iteration scheme which will always converge provided an iteration parameter is properly chosen:

$$\begin{aligned} \mathcal{S}_p^0 &= 0, \\ \text{For } k = 0, 1, 2, \dots, \text{ find } (\phi_h^{k+1}, v_h^{k+1}) &\in \mathring{H}^1 \times \mathring{H}^1 \text{ so that} \\ C_1 \left((\phi_h^{k+1})', \psi' \right) + (\phi_h^{k+1}, \psi) &= \langle p, \psi \rangle - C_2 (\mathcal{S}_p^k, \psi), \quad \text{for all } \psi \in S^h, \\ \left((v_h^{k+1})', \eta' \right) &= (\phi_h^{k+1}, \eta), \quad \text{for all } \eta \in S^h, \\ \mathcal{S}_p^{k+1} &= \mathcal{S}_p^k + \omega \left(\int_0^L v_h^{k+1}(x) dx - \mathcal{S}_p^k \right). \end{aligned} \quad (4.11)$$

5. SOME COMMENTS ON IMPLEMENTATION AND THE NONLINEAR PROBLEM

In this section, we note some observations on the implementation of the methods proposed in Sections 3 and 4. For a three span continuous bridge, as mentioned earlier, the conforming finite element method requires $S_c^h \subseteq C^2(0, \ell)$ and also that the functions in S_c^h vanish at $x = 0, \ell$, and the tower nodes. This can easily be accomplished using cubic B-splines, and “adjusting” the basis functions near the nodes at the ends of the spans. The iterative scheme for this problem is seen to be

$$\begin{aligned} \text{Find } v_h^{k+1}(x) &\in S_c^h \text{ so that} \\ C_1 \left((v_h^{k+1})'', \phi'' \right) + \left((v_h^{k+1})', \phi' \right) &= \langle p, \phi \rangle - C_2 (\mathcal{S}_p^k, \phi), \quad \text{for all } \phi \in S_c^h, \end{aligned} \quad (5.1)$$

where \mathcal{S}_p^k is updated as in (4.2) or (4.11). The stiffness matrix generated in (5.1) is the same for each iteration, and hence can be formed at the beginning of the procedure and factored using a banded LU factorization (see, e.g., [15]). Since \mathcal{S}_p^k is a constant at each step of the iteration, the updating step in (5.1) simply involves subtracting a constant from each entry in the forcing vector (although again some adjustment is required near the boundary nodes). The computation of the new \mathcal{S}_p^k requires integrating the solution $v_h^k(x)$, which is trivial to do (especially if a uniform grid is used). The new $v_h^{k+1}(x)$ is then computed from (5.1) by forward and backward solving the entire (factored) system.

Similar comments hold for the mixed finite element method: here, S^h may be taken to be piecewise linear functions which vanish at the ends of each span. The stiffness matrices formed by (4.2) or (4.11) are tridiagonal, and can easily be factored into LU form, resulting in a very fast method. Whereas for a three span model the equations for the conforming method are “coupled,” due to the C^2 continuity requirement across the tower nodes, the system for the mixed method can be solved as three independent sets of equations (the \mathcal{S}_p^k term is of course global), and

numerical experiments indicate that increased rates of convergence for the iteration method can be achieved if S_p^k is updated after the solution on each span has been computed. Numerical experiments also indicate that the bounds on C_2 and L in Theorem 4.1 and ω in Theorem 4.2 are not sharp, but that the methods (4.2) and (4.11) are highly unstable if H_g is not large enough in (4.2) or ω is not small enough in (4.11).

Although we presented no existence/uniqueness proofs for the nonlinear model (1.1), it is easy to modify the above numerical schemes to approximate the solution of the equation (assuming this solution exists). The main problem is that the stiffness matrix generated in the iteration cycles will now depend on S_p^k , and as such must be recomputed for each iteration. For the mixed method this is only a minor impediment, but the computational process is slowed considerably for the conforming method. Some computational results for the nonlinear problems appear in Section 6.

In general, the iteration procedures presented here can be easily incorporated into existing finite element codes for both the mixed and conforming models. The flexibility of these methods in dealing with various loading functions, and even variable coefficient problems makes up for the added computational effort.

6. NUMERICAL EXPERIMENTS

In this section, we implement the methods proposed in Sections 3 or 4 on several test problems. The first experiment is designed to check the efficiency of the iterative process given by (4.11) and also the error bounds given in Theorems 3.1 and 3.2. We consider equation (2.1), with $C_1 = C_2 = L = 1.0$; a solution of the form

$$v(x) = G_1 x + G_2 e^x + G_3 e^{-x} + x^3, \quad (6.1)$$

was chosen (G_1 , G_2 , and G_3 chosen so that $v(x)$ satisfies the boundary conditions), and subsequently $p(x)$ was computed by (2.1). Rewriting the problem as the system (2.7), the mixed finite element method (3.12) was then used to approximate the system. A uniform mesh was used, and the approximation space S^h was taken to be the standard space of piecewise linears. To start, the mesh sized was fixed at $h = 0.01$, and the scheme given by (4.11) was used to solve the equations. The method was iterated until $|S_p^{k+1} - S_p^k| < 10^{-6}$, and various ω were used. Figure 2 shows a plot of ω versus the number of iterations required to attain the cutoff tolerance (the method did not converge for $\omega = 2.0$).

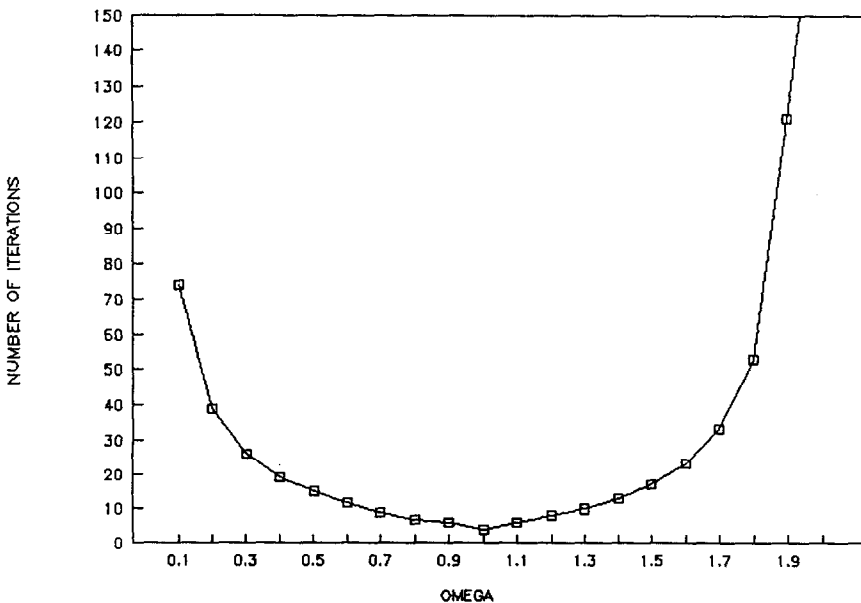


Figure 2. Number of iterations vs. omega; linear hinged model.

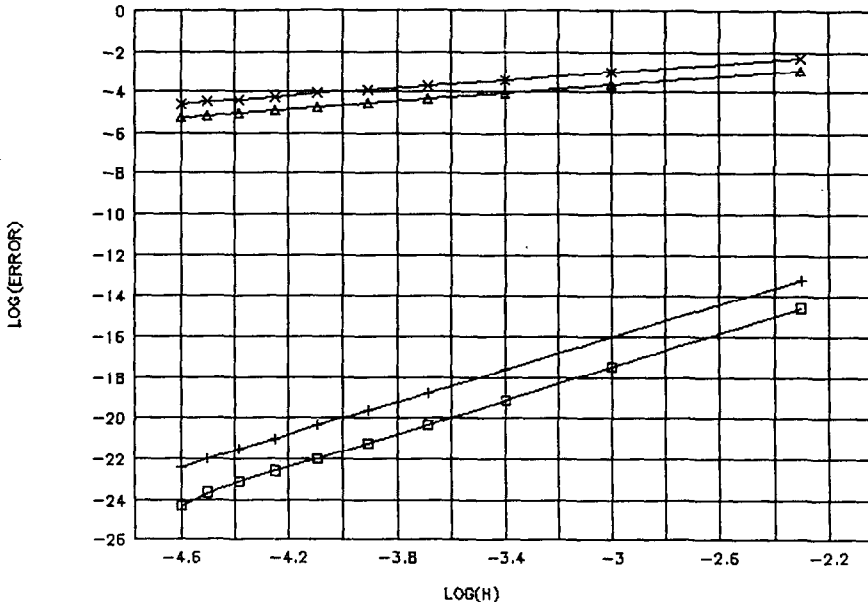


Figure 3. Finite element error vs. mesh size on log-log scale: \times = line of slope 1, Δ = error in energy norm, hinged linear model, $+$ = line of slope 4, \square = integral error; continuous linear model.

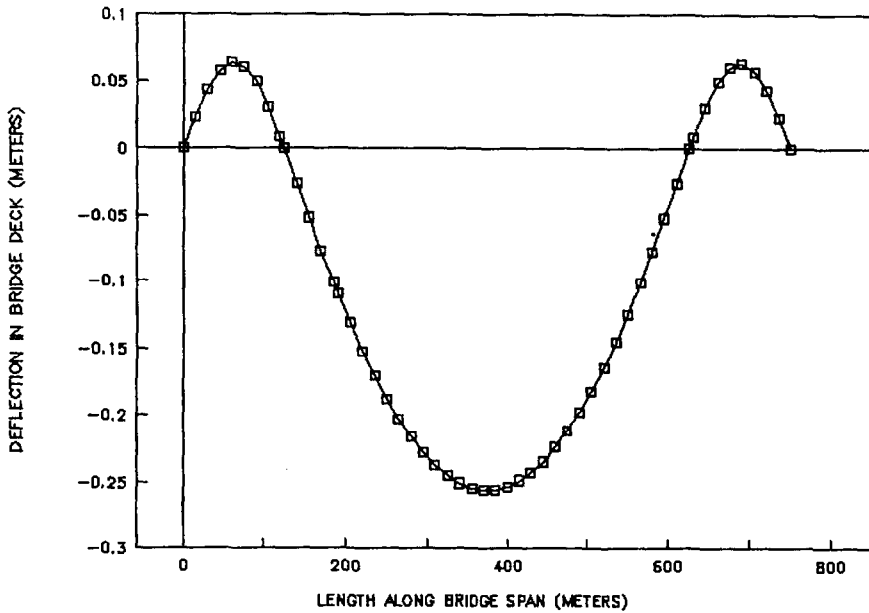


Figure 4. Bridge deflection under local live load; linear hinged model.

As a further analysis of this test problem, the mesh size was varied and the error $\|\phi - \phi_h\|_1 + \|v - v_h\|_1$ was computed for each run. The above cutoff tolerance was used and ω was fixed at 1.0. The same problem was then approximated using the continuous model (3.4), with S_c^h taken to be the space of cubic B-splines on a uniform mesh, and the integral error (3.6) was computed for various mesh sizes. Both of these errors are plotted on a log-log scale in Figure 3, along with reference lines of slope one and four. The results clearly show the $O(h)$ and $O(h^4)$ convergence rates predicted by Theorems 3.1 and 3.2.

For the remaining experiments, a model "benchmark" three-span suspension bridge (see [6]) was used: the lengths of the spans are taken to be 125 m - 500 m - 125 m, and the dead weight load of the bridge deck is $w = 127$ kN/m. The resulting dead load horizontal tension in the cables is taken to be $H_g = 91,969$ kN. The cross sectional area of the cables is taken to be 0.28 m²,

$E = 206 \times 10^6 \text{ kN/m}^2$, $E_c = 157 \times 10^6 \text{ kN/m}^2$, and $I = 1.5 \text{ m}^4$ for all three spans. The length L_c was taken to be 900 m.

The next experiment measured the actual deflection in the bridge spans under a uniform loading. The hinged model was used, and the computations were done using the mixed finite element formulation on a uniform grid of size $h = 0.1$. The resulting system of equations was solved using the iteration scheme (4.11). The load was taken to be 10 kN, and was applied to the middle span only. This results in a downward deflection of the middle span, and (due to the global cable tension term) an upward deflection of the side spans. The maximum deflection of the side spans occurred 62.5 m from the bridge ends (i.e., the center of the side spans) and was computed to be 0.064 m. The maximum deflection of the middle span occurred at a point 375 m from the end points (i.e., at the midpoint of the bridge), and was computed to be 0.2564 m. For this size load, the linear model gives an accurate approximation to the nonlinear model (see next experiment). A plot of the bridge deflection is shown in Figure 4. Data points were plotted every 15 m along the bridge deck.

The purpose of the next experiment was to explore the difference between the linear and nonlinear models for the bridge. The hinged model (3.12) was again used, and the approximation was done on a uniform mesh of size $h = 0.1$ with a piecewise linear approximation space. The iteration scheme (4.11) was again used, this time with a relative cutoff tolerance of

$$\frac{|S_p^{k+1} - S_p^k|}{|S_p^k|} < 10^{-4}. \quad (6.2)$$

It was found after some experimentation that $\omega = 0.14$ had a rapid rate of convergence for both the linear and nonlinear equations. The load $p(x)$ was taken to be constant throughout the bridge, and numerous runs were made for various $p(x)$. The maximum deflection in the bridge was computed (naturally occurring at the middle of the bridge), and a relative difference between the linear and nonlinear models was computed, i.e.,

$$\frac{|\text{max deflection nonlinear} - \text{max deflection linear}|}{\text{max deflection nonlinear}}. \quad (6.3)$$

These relative differences are shown in Figure 5. The numbers indicate that even for live loads approaching the weight of the bridge deck itself, the relative difference between the two models is less than 7%.

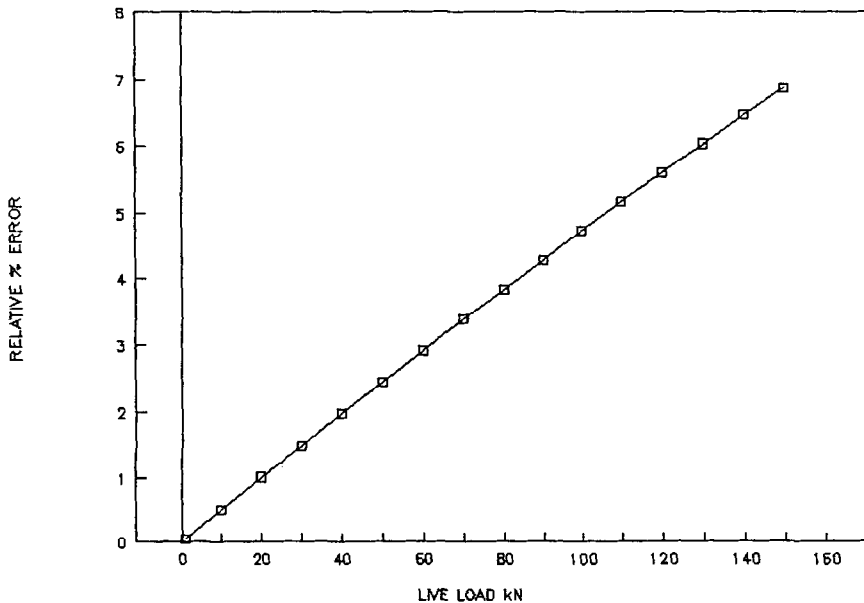


Figure 5. Relative error between linear and nonlinear hinged models vs. live load.

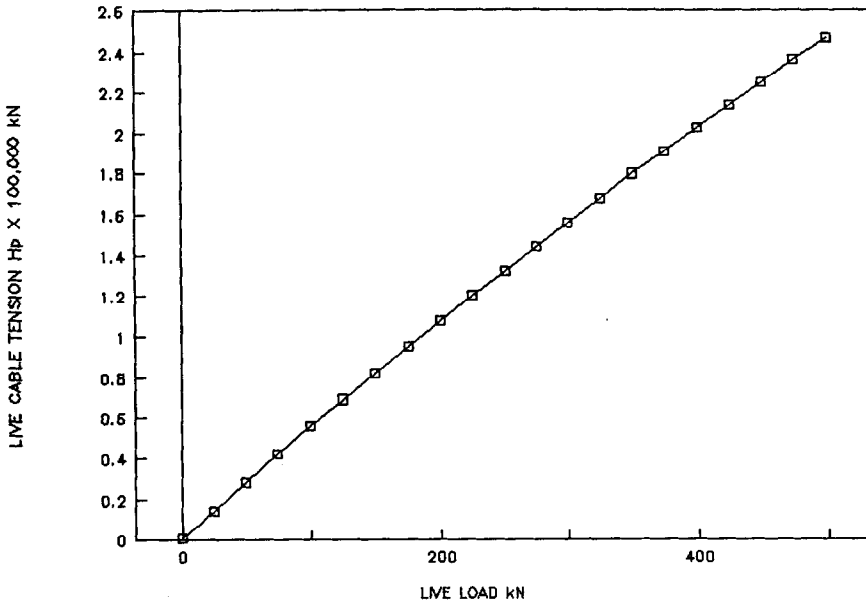
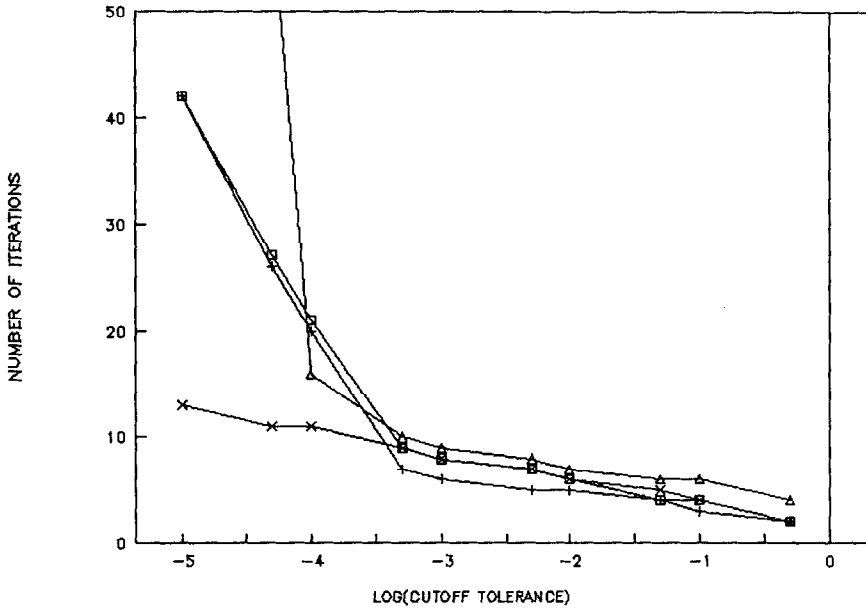


Figure 6. Live cable tension vs. live load; nonlinear hinged model.

Figure 7. Number of iterations for convergence vs. log of cutoff tolerance: \times = continuous linear model, Δ = continuous nonlinear model, $+$ = hinged nonlinear model, \square = hinged linear model.

To further explore the nonlinear model, the above experiment was run again with various live loads, and the live cable tension H_p was computed from the numerical model. The results are shown in Figure 6, and indicate that the nonlinear model behaves almost linearly even for very large live loads—thus the assumption that the linear model is a good approximation seems justifiable in the case of static deflection.

For a final experiment, the above bridge was loaded with a local live load given by the function

$$p(x) = \begin{cases} 100, & 325.0 \leq x \leq 425.0, \\ 0, & \text{else.} \end{cases} \quad (6.4)$$

The mesh was fixed at $h = 0.1$, and the linear and nonlinear mixed methods (3.12) were computed using the scheme (4.11) with $\omega = 0.1$ and various relative cutoff tolerances. In addition, the linear

and nonlinear conforming methods (3.4) were also approximated with the same ω and cutoff tolerances. Figure 7 shows the total number of iterations required for convergence for each model versus the cutoff tolerance used to decide convergence. Note that the conforming linear model actually converged rather quickly, but that the nonlinear conforming model did not converge at all for tolerances less than approximately 10^{-4} . Various other ω choices were tried, but the nonlinear conforming method could not be made to converge.

7. CONCLUSIONS

This work explored two straightforward finite element methods for approximating the solution of a fourth order integro-differential equation which is used to model static deflection in suspension bridges. In addition to showing error estimates for these methods, an iterative method was introduced to find the numerical solution which did not involve forming the entire stiffness matrix (which would be partly or totally full due to the integral term). These methods can be implemented by modifying standard finite element software, and thus offer all the flexibility of the finite element method. Numerical experiments indicate that the linear model is a good approximation to the nonlinear equation, even under rather large live loads. Further research is being done on the nonlinear problem; one such model utilizes the Timoshenko beam model for the stiffening girders, thus allowing for shear deformation. However, it seems clear that any model which is to be used to analyze large scale oscillations will need to remove the assumption of unextendible cables, as in the Lazur-McKenna model.

REFERENCES

1. J. Melan, Theorie der eisernen Bogenbrücken und der Hängebrücken, In *Handbuch der Ingenieurwissenschaften*, Vol. 2, Part 4, Wilhelm Engelmann, Leipzig, (1888).
2. A.C. Lazur and P.J. McKenna, Large amplitude periodic oscillations in suspension bridges: Some new connections with nonlinear analysis, *SIAM Review* **32** (4), 537–578 (December 1990).
3. Y.S. Choi, K.C. Jen and P.J. McKenna, The structure of the solution set for periodic oscillations in a suspension bridge model, *IMA J. Appl. Math.* **47**, 283–306 (1991).
4. A. Pugsley, *The Theory of Suspension Bridges*, 2nd Ed., Edward Arnold Pub. LTD, London, pp. 75–92, (1968).
5. T. von Karman and M.A. Biot, *Mathematical Methods in Engineering*, 1st ed., pp. 277–283, McGraw-Hill, (1940).
6. H. Ohshima, K. Sato and R. Watanabe, Structural analysis of suspension bridges, *J. Engr. Mech.* **110** (3), 392–404 (March 1984).
7. G. Fairweather and R.D. Saylor, The reformulation and numerical solution of certain nonclassical initial-boundary value problems, *SIAM J. Sci. Stat. Comput.* **12** (1), 127–144 (Jan 1991).
8. B. Semper, Locking in finite element approximation of long thin extensible beams, *IMA Jour. of Num. Anal.* (to appear).
9. I. Babuska, Error bounds for the finite element method, *Numer. Math.* **16**, 322–333 (1971).
10. F. Brezzi, On the existence, uniqueness, and approximation of saddle point problems arising from Lagrangian multipliers, *RAIRO Anal. Numer.* **8**, 129–151 (1974).
11. J.E. Roberts and J.M. Thomas, Mixed and hybrid methods, In *Handbook of Numerical Analysis: Part 1: Finite Element Methods*, (Edited by P.G. Ciarlet and J.L. Lions), North-Holland, Amsterdam, 523–641, (1991).
12. F. Brezzi and M. Fortin, *Mixed and Hybrid Finite Element Methods*, Springer-Verlag, (1991).
13. C. DeBoor, *A Practical Guide to Splines*, Springer-Verlag Applied Math. Sciences Series, Springer-Verlag, (1978).
14. P.G. Ciarlet, Basic error estimates for elliptic problems, In *Handbook of Numerical Analysis Part 1: Finite Element Methods*, (Edited by P.G. Ciarlet and J.L. Lions), North-Holland, Amsterdam, (1991).
15. G. Golub and C. Van Loan, *Matrix Computation*, 2nd Ed., Johns Hopkins Press, Baltimore, (1989).